magnetochemistry

MDPI

Article

Interrelation between the Solid-State Synthesis Conditions and Magnetic Properties of the $NiCr_2O_4$ Spinel

Mikhail Cherosov, Ruslan Batulin *, Airat Kiiamov, Alexey Rogov, Iskander Vakhitov, Damir Gabadullin, Dmitrii Tayurskii and Roman Yusupov

Institute of Physics, Kazan Federal University, Kremlyovskaya Str., 18, 420008 Kazan, Russia
* Correspondence: tokamak@yandex.ru

Abstract: The synthesis of the $NiCr_2O_4$ compound with the spinel structure via the high-temperature solid-state reaction leads to different deviations of the cationic composition from the nominal depending on the atmosphere in the furnace chamber. The samples prepared from the same starting NiO and Cr_2O_3 compounds but in different atmospheres differ in phase composition and orbital and spin ordering temperatures. We find that a common route of synthesis in the air and a possible presence of the Ni_2O_3 in initial NiO lead to the incorporation of the Ni^{3+} ions into the octahedral sites regularly occupied by the Cr^{3+} ions. This results in a decrease in the orbital ordering and an increase in the Nèel temperatures. We propose that the Nèel temperature value serves as a measure of a departure of a composition from the nominal $NiCr_2O_4$. The lowest Nèel temperature among our series was T_N = 63 K which we consider the closest to the intrinsic quantity of the $NiCr_2O_4$ compound.

Keywords: spinel structure; solid-state synthesis; cationic composition; critical temperature

check for updates

Citation: Cherosov, M.; Batulin, R.; Kiiamov, A.; Rogov, A.; Vakhitov, I.; Gabadullin, D.; Tayurskii, D.; Yusupov, R. Interrelation between the Solid-State Synthesis Conditions and Magnetic Properties of the $NiCr_2O_4$ Spinel. *Magnetochemistry* **2023**, *9*, 13. https://doi.org/10.3390/magnetochemistry9010013

Academic Editors: Devashibhai Adroja and Dmitry Alexandrovich Filippov

Received: 11 November 2022
Revised: 23 December 2022
Accepted: 26 December 2022
Published: 30 December 2022

Copyright: © 2022 by the authors. Licensee MDPI, Basel, Switzerland. This article is an open access article distributed under the terms and conditions of the Creative Commons Attribution (CC BY) license (https://creativecommons.org/licenses/by/4.0/).

1. Introduction

Crystalline materials with the spinel structure and a general chemical formula MM'_2X_4 are studied for several decades due to a broad range of magnetic, structural, and dielectric properties [1–9]. Typically, M and M' are metal ions or a combination of them, and X represents oxygen or some chalcogen divalent anion (S^{2-}, Se^{2-}, Te^{2-}). Among spinels, oxide compounds reveal outstanding mechanical properties (hardness) and high-temperature stability. Two types of cationic positions are present in spinels: tetrahedrally coordinated A-sites and octahedrally coordinated B-sites. Cations in the B-sites form a network of corner-sharing tetrahedra, typical for pyrochlores. Each face of a regular tetrahedron represents an equilateral triangle. If the B-sites are occupied by the magnetic ions with an antiferromagnetic coupling in each pair, B-sublattice is the subject of magnetic frustration. When Cr^{3+} ions reside at the B site, the material is known as chromite. $ZnCr_2O_4$ [10] and $MgCr_2O_4$ [11] chromites are prominent representatives of frustrated magnets.

In recent decades, much attention has been paid to transition metal chromites, when both A and B sites are occupied by magnetic ions [12,13]. In these compounds, a sequence of magnetic phase transitions takes place. In some cases, spontaneous polarization development accompanies these transitions, and a multiferroic state is formed. Thus, in $CoCr_2O_4$ a polar state appears with an onset of a spiral modulation of ferrimagnetic structure [14]. Multiferroics are promising in practical applications for the creation of magnetic non-volatile memory elements where the information is written by an electric field.

For $FeCr_2O_4$, electric polarization is induced by an applied electric field above the Nèel temperature T_N and is metastable [15]. Among transition metal chromites, nickel chromite $NiCr_2O_4$ attracts much attention due to manifestations of multiferroicity, pronounced magnetodielectric, and magnetostrictive phenomena. Moreover, $NiCr_2O_4$ has diverse promising applications such as catalyst materials [16,17], electrodes in supercapacitors [18], sensitive gas sensors [19], etc.

Nickel chromite $NiCr_2O_4$ is a normal spinel with a cubic structure slightly above room temperature [20]. The ground state of the Ni^{2+} ions in a regular tetrahedral surrounding is the orbital triplet. Consequently, at $T_{OO} \approx 310$ K the nickel chromite spinel experiences the second-order phase transition to an orbitally ordered state. Orbital ordering occurs in the Ni-ion A-site sublattice, and crystal structure symmetry is lowered to tetragonal. On cooling to ~ 70 K, the symmetry of the $NiCr_2O_4$ crystal structure is further lowered to orthorhombic, almost simultaneously with an onset of the ferrimagnetic order at T_N ~ 65 K [21,22]. On cooling below 40 K, the magnetic order develops further which is manifested in a jump of magnetization at T_s ~ 31 K [23,24]. The magnetic structure of $NiCr_2O_4$ is considered a superposition of ferrimagnetic (longitudinal) and antiferromagnetic (transverse) counterparts, and the latter sets in at T_s [23–27].

However, the complex magnetic structure of chromite spinels is still under debate. $NiCr_2O_4$ spinels require careful verification that the samples under study correspond to the declared stoichiometry. It is expected and verified experimentally that a dilution of the chromium sublattice with guest ions disturbs the magnetic frustration and thus leads to an increase in the Nèel temperature [28–31]. Our recent studies show that the substitution of the chromium sublattice of $FeCr_2O_4$ spinel can also occur in an uncontrolled manner due to the oxidation of Fe^{2+} ions to the Fe^{3+} state [32].

Summarizing, one can generally state that deviations of complex magnetic spinels, and transition metal chromites in particular, from their nominal compositions, can easily lead to wrong and misleading interpretations of the obtained experimental data. For practical applications, it is highly desirable to have an easily controlled criterion that would indicate a deviation from the nominal composition of a compound. In the case of iron chromite, Mössbauer spectroscopy of iron nuclei has shown itself a powerful experimental approach sensitive both to iron-ions coordination and oxidation state [33]. In the case of nickel chromite, the use of the Mössbauer effect is in principle possible (for ^{61}Ni nuclei with a natural abundance of 1.1%). However, this requires experiments with synchrotron radiation, which limits its use as an express method.

In this paper, the studies of $NiCr_2O_4$ polycrystalline powder samples with spinel structure are presented. We show that the atmosphere in a furnace chamber in the course of a conventional high-temperature solid-state synthesis affects notably the resulting composition of an output product. We analyze the output phase composition as well as the elemental composition of the spinel fraction, its magnetic properties, and critical temperatures of the spin and orbital orderings. It will be shown that all three critical temperatures T_{OO}, T_N and T_s vary with changing the synthesis atmosphere. We suggest that the value of the Nèel temperature can serve a criterion for a departure of a nickel chromite spinel from the nominal $NiCr_2O_4$.

2. Sample Preparation and Experimental Details

A series of seven polycrystalline $NiCr_2O_4$ samples (Table 1) was synthesized by the high-temperature solid-state reaction procedure using the nickel (II) oxide NiO (99.95% from Lanhit Ltd., Moscow, Russia) and chromium (III) oxide Cr_2O_3 (99.5% from Alfa Aesar, Haverhill, MA, USA). The reagents were dried at the temperature of 250 °C for 12 h in the air, mixed in a target ratio (in the majority of cases, stoichiometric), and thoroughly ground in an agate mortar for 3 h. The synthesis was performed in the vertical tube furnace (GSL1700X, MTI, Richmond, VA, USA) with the mixture kept in an alumina crucible. Several syntheses were carried out with various atmospheres in the furnace chamber—in the air (samples I and II), in an argon flow (sample III), in a steady mixture of 90% of Ar and 10% of air (sample IV) or in the steady nitrogen (samples V–VII). In a case of an argon or nitrogen atmosphere, the chamber was evacuated to 10^{-2} mbar and purged with the pure Ar/N_2 gas (99.9998%) several times. Then the synthesis took place in either a weak flow of argon (~0.01 L/min) or a sealed chamber with a slight overpressure (~0.02–0.03 bar) of Ar,

Ar/air mixture or N_2-gas at a temperature of 1200 °C or 1300 °C for 24 h. The synthesis was supposed to follow the reaction of

$$NiO + Cr_2O_3 \rightarrow NiCr_2O_4 \quad (1)$$

Table 1. A list of the $NiCr_2O_4$ powder samples obtained by the solid-state synthesis procedure, conditions of the synthesis, products of the reaction according to XRD data, and temperature of the orbital ordering T_{OO}.

Sample	Atmosphere	Synthesis Temperature, Deg. C	Molar Ratio Cr_2O_3/NiO in Initial Mixture	Products	T_{OO}, K
I	Air	1200	1:1	spinel (92%), Cr_2O_3 (8%)	<295
II	Air	1200	1:1.1	spinel (99.8%), Cr_2O_3 (0.2%)	<295
III	Ar flow	1200	1:1	spinel (65%), Cr_2O_3 (8%), Ni (27%)	>295
IV	Air (10%)+ Ar (90%) closed	1200	1:1	spinel (99.3%), Cr_2O_3 (~0.7%)	<295
V	N_2 closed	1200	1:1	spinel (67%), Cr_2O_3 (22%), NiO (11%)	>295
VI	N_2 closed	1300	1:1	spinel (99.6%), Cr_2O_3 (0.4%)	313
VII	N_2 closed	1300	1:1	spinel (99.6%), Cr_2O_3 (0.4%)	>295

Note that the synthesis in a nitrogen atmosphere demanded an elevated temperature of 1300 °C (samples VII and VIII) as its performance at 1200 °C left a significant part of an initial mixture unreacted (sample VI).

The resulting product in all cases was examined for a formation of the desired phase as well as the impurity phases with the powder XRD analysi. XRD measurements were carried out with the Bruker D8 Advance diffractometer (Bruker AXS GmbH, Karlsruhe, Federal Republic of Germany) equipped with the Cu-Kα source. Due to imperfect spectral filtering of the X-rays, each diffraction maximum has a doublet structure originating from the Kα1 and Kα2 components. Prior to measurements, samples were carefully ground in an agate mortar to a fine powder state. The temperature of a sample was stabilized with the nitrogen vapor flow system (Anton Paar, Graz, Austria).

The morphology of the obtained samples was studied with scanning electron microscopy (SEM). The images were taken with the Merlin (Carl Zeiss, Oberkochen, Federal Republic of Germany) high-resolution self-emission microscope at a low acceleration voltage of 5 kV in the secondary electron detection mode. A sample was dispersed over a carbon tape and covered with 10 nm of AuPd 80/20 alloy using the Q150T ES (Quorum Technologies, Lewes, UK) sample preparation system. Elemental analysis was performed by means of energy-dispersive spectrometry (EDX) with the X-Max setup (Oxford Instruments, Abingdon-on-Thames, UK) combined with SEM, at an accelerating voltage of 20 kV.

Magnetization measurements of the samples were performed with vibrating sample magnetometry (VSM) option of the Physical Property Measurement System PPMS-9 (Quantum Design, San Diego, CA, USA) in a temperature range of 5–300 K and the magnetic fields within $\pm$ 9 T. Temperature dependences of the susceptibility were studied under an applied field of 10 mT.

Further, the results for the four characteristic representatives of the series, namely, samples I, II, III, and VI, will be presented and discussed.

3. X-ray Diffraction Analysis

Powder XRD patterns of the synthesized $NiCr_2O_4$ samples I, II, III, and VI at room temperature (RT) are presented in Figure 1. Diffractograms of samples I and II produced in the air reveal an occurrence of two crystalline phases—a dominant cubic-symmetry spinel and a residual α-Cr_2O_3. For sample I, the phase's contents were 92% and 8%, and for sample II, these were 99.8% and 0.2%, respectively. A modification of the NiO/Cr_2O_3 mixture composition from stoichiometric (see Table 1) by an excessive 10 mol.% of NiO was done intentionally to compensate for an assumed loss of NiO in the course of a synthesis. This trick has indeed led to essentially a single-phase spinel-structure product. However, the masses of an initial NiO/Cr_2O_3 mixture and of a product were identical indicating no loss of NiO. It means that nickel ions somehow substitute partially for Cr^{3+}-ions in the B-sites of the spinel.

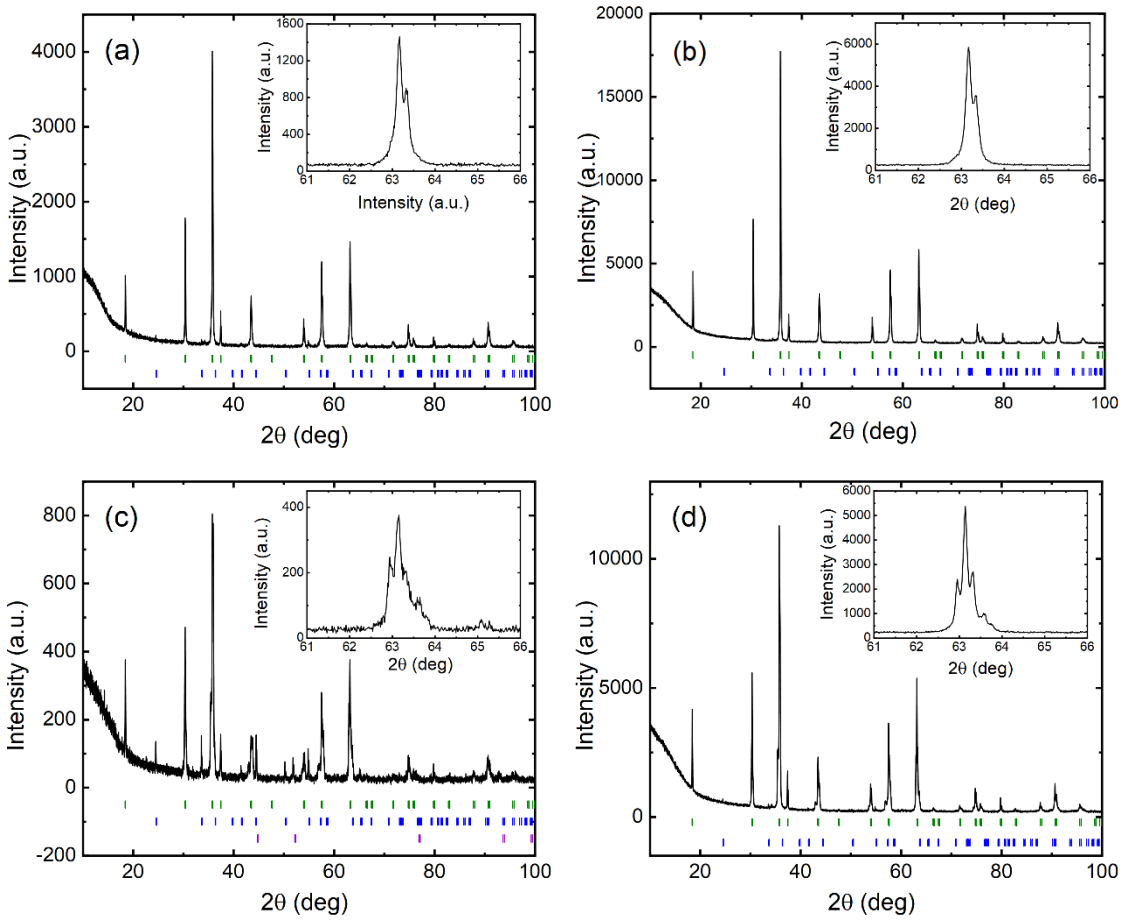

Figure 1. Powder XRD patterns of samples I (**a**), II (**b**), III (**c**), and VI (**d**) measured at T = 295 K. Vertical tick patterns represent Bragg peak positions of the $NiCr_2O_4$ (green), Cr_2O_3 (blue), and nickel (purple) constituents. Insets show the XRD pattern in the 2θ angle range corresponding to the (440) maximum of the cubic spinel phase (see text).

The diffractogram of sample III (Figure 1c) synthesized in a flow of argon, at room temperature, reveals four crystalline phases: two spinel phases—one with the cubic and another with the tetragonal symmetry (in total 65%), metallic nickel (27%), and a residue of α-Cr_2O_3 (8%). Evidently, an exposure of NiO to the high temperature of 1200 °C results in a chemical reduction of nickel to the metallic state that cannot participate in the reaction

with Cr_2O_3. A presence of the tetragonal-structure spinel fraction is expected as at ~ 310 K an orbital ordering in the Ni-ion sublattice sets in.

Sample VI was synthesized with the oven chamber filled with nitrogen without its flow. Its diffractogram contains the patterns of three crystalline phases: two spinel-structure ones similar to sample III (in total 99.5%), and a vanishingly small amount of α-Cr_2O_3 (0.5%).

Temperature transformation of the XRD pattern of sample VI was studied in a limited 2θ-range from 61 to 66 degrees (Figure 2). In this range, the (440) diffraction maximum of the cubic $NiCr_2O_4$ phase is located, which splits into the (224) and (400) peaks below the structural phase transition temperature. The symmetry lowering is due to the cooperative Jahn-Teller effect within the A-ion (Ni^{2+}) sublattice. At T = 323 K and above, a single (404) diffraction maximum is observed which corresponds to the cubic $Fd\bar{3}m$ phase of $NiCr_2O_4$. On cooling (Figure 2), new components start to manifest themselves on the left and right wings of the cubic-phase (404) peak while the last gradually vanishes. The development of the diffraction pattern indicates a coexistence of the cubic and tetragonal phases in the temperature range of 288–313 K; below 288 K, the sample reveals only the tetragonal I41/amd phase. Such an observation shows that the actual sample is not perfectly homogeneous and is characterized by a distribution of the critical orbital ordering temperatures.

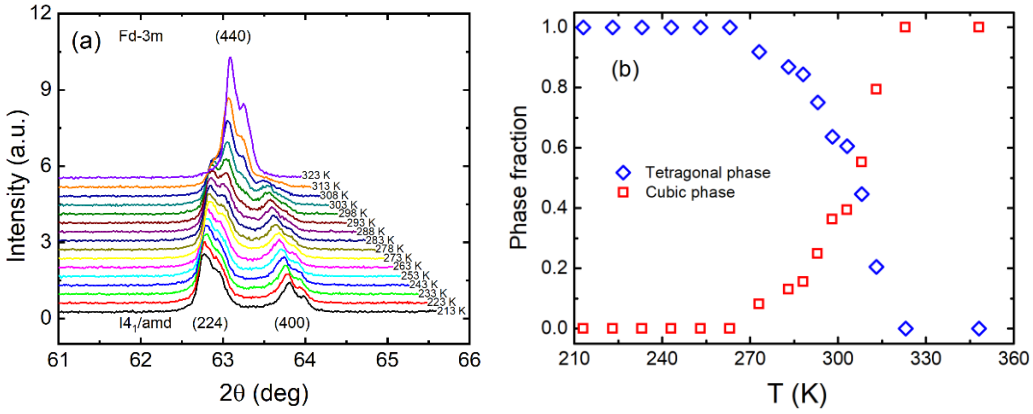

Figure 2. (**a**) Temperature dependence XRD pattern of the powder $NiCr_2O_4$ sample VI in the course of the structural phase transition associated with an orbital ordering within the Ni^{2+} A-site sublattice, (**b**) Temperature dependence of the cubic- (squares) and tetragonal-symmetry (triangles) phase fractions.

The patterns in the 2θ-range of 61–66 degrees measured at T = 295 K for samples I, II, III, and VI are shown in the insets to panels (a)–(d) of Figure 1, respectively. Clearly, samples I and II are found fully within the whole volume in the cubic phase while samples III and VI represent the mixtures of the cubic and tetragonal-symmetry phases. Thus, we can conclude that samples I and II have $T_{OO} < 295$ K. This indicates that samples I and II, on one hand, and III and VI, on the other, are different.

4. Morphology and Chemical Composition

In Figure 3a–d, the SEM images of the $NiCr_2O_4$ powder samples I, II, III, and VI are presented. Samples I and II synthesized in the air evidently have larger mean grain size than samples III and VI obtained in a flow of argon and in a steady N_2 atmosphere, respectively. Most of the grains in the obtained powders have a characteristic for spinels octahedron-like shape. Grain images for samples I, II, and VI are very clear and high-contrast, however, an image of sample III is notably worse. This is a consequence of a multi-phase composition of sample III with comparable fractions of a spinel, Cr_2O_3, and metallic nickel (Table 1). Definitely, the grains of sample III have a developed surface and probably are covered with the impurity phases.

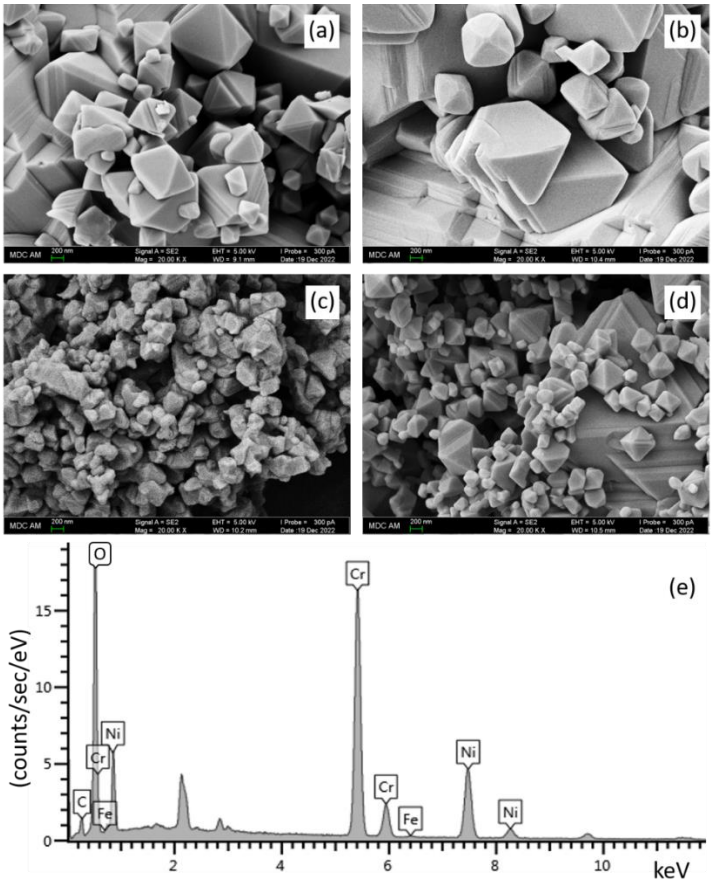

Figure 3. Scanning electron microscopy images of $NiCr_2O_4$ powder samples I (**a**), II (**b**), III (**c**), and VI (**d**). Energy dispersion spectrum of sample II (**e**).

A typical EDX spectrum (sample II) of the obtained materials is shown in Figure 3e. We have extracted from these spectra a ratio of Ni:Cr concentrations (Table 2). For samples, I, II, and VI, these ratios are well-defined regardless of a chosen grain/spot. The concentration of chromium in all three samples is less than twice the concentration of nickel. The Ni:Cr ratio of sample III varies in a broad range from 1:2.2 to 1:9 depending on a spot. This shows that the Cr_2O_3 dominates at the surface of the spinel grains in this multi-phase sample. The knowledge of the Ni:Cr ratio allows us to calculate the substitution degree x of the Cr^{3+}-sites by nickel-ions assuming the composition of the spinel phase as $Ni(Cr_{1-x}Ni_x)_2O_4$.

Table 2. Cationic composition Ni:Cr and a substitution degree x of the Cr^{3+} sites by nickel ions in $Ni(Cr_{1-x}Ni_x)_2O_4$ and magnetic critical temperatures T_N and T_s determined from VSM data.

Sample	Ni:Cr Ratio	x, at.%	T_N, K	T_S, K
I	1:1.98	0.3	68.5	25.7
II	1:1.85	2.6	73.1	22.3
III	1:(2.18 to 9)	0 *	63.0	27.2
VI	1:1.97	0.5	67.7	25.8

* an assumed value, see the text.

5. Magnetic Properties of $NiCr_2O_4$ Powder Samples

Figure 4 shows the temperature dependences of the magnetization of samples I, II, III, and VI measured on cooling in the field of 10 mT. For sample III, ferromagnetic nickel particles have been extracted from the powder with the permanent NdFeB magnet prior to measurements. M(T) curves of every sample reveal two anomalies. The first anomaly

corresponds to the transition from the paramagnetic to the ferrimagnetic state at T_N. Nèel temperature for samples I, II, III, and VI has the value of 68.5 K, 73.1 K, 63.0 K, and 67.7 K, respectively (Table 2). On further cooling, a rise of magnetization is observed at T_s associated with the antiferromagnetic counterpart of the magnetic structure due to a long-range ordering in the transverse spin arrangement [23–27]. This anomaly takes place at 25.7 K, 22.3 K, 27.2 K, and 25.8 K for samples I, II, III, and VI, respectively. Note an obvious correlation between the trends for two magnetic transitions: the lower the Nèel temperature the higher the T_s. Thus, we find that the magnetic ordering in the four representatives of our series that differ in the synthesis conditions takes place at different temperatures again indicating some differences in these samples.

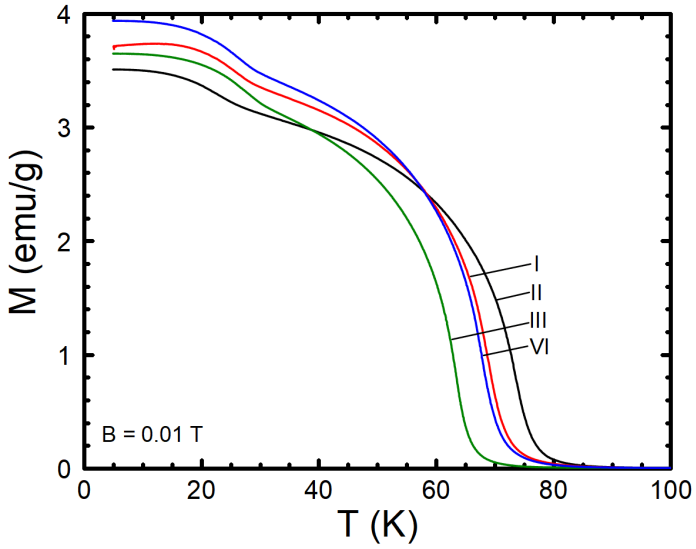

Figure 4. Temperature dependences of the magnetization of samples I, II, III, and VI of the $NiCr_2O_4$ powders measured with an applied magnetic field of 10 mT on cooling.

Magnetization curves were also studied to compare the coercivities and saturation magnetizations of $NiCr_2O_4$ powders. Figure 5 shows hysteresis loops measured at 40 K ($T_s < T < T_N$) and at 10 K ($T < T_s$) for samples II, III, and VI. For each sample, the coercive field value is ~0.25 T at 40 K and ~0.54 T at 10 K. The loops of all samples are near identical, only the saturated magnetic moment for sample II is ~ 10% less than that of samples III and VI. Moreover, a non-monotonous variation of the magnetization is found for sample II on changing the sign of an applied field revealing the presence of another magnetic fraction.

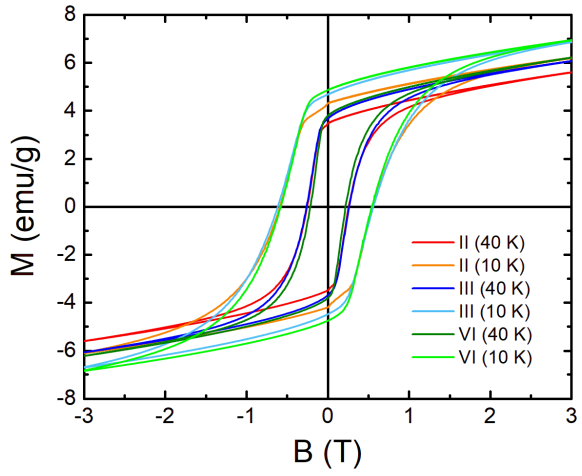

Figure 5. Magnetic hysteresis loops of samples II, III, and VI measured at T = 10 K and at T = 40 K.

6. Discussion

Four representatives of a series of nominal $NiCr_2O_4$ powders with the spinel structure that were produced by the high-temperature solid-state synthesis from the same NiO and Cr_2O_3 oxides differ in values of three critical temperatures characteristic for the target compound. What can serve as a source for these differences? A clue, in our opinion, lies in (i) a need for an extra 10 mol.% of NiO to obtain a phase-pure spinel-structure product (sample II, Table 1) and (ii) a non-stoichiometric ratio of Cr:Ni < 2 for samples I, II, and VI (Table 2). This clearly indicates a partial substitution of the octahedral Cr^{3+}-sites by nickel ions.

To our knowledge, no cationic disorder was reported for the $NiCr_2O_4$ compound. Such substitution could happen if NiO contains Ni^{3+} ions. An easy transformation of NiO to Ni_2O_3 is well known and manifests itself in the color change of naturally green NiO to black "nickel oxide". Indeed, the starting NiO that we used for the synthesis had a greyish-greenish color. Though the XRD test had not revealed any crystalline constituent apart from the cubic NiO in it, X-ray photoemission indicates only Ni^{3+} ions at the surface of the particles. Thus, at least a presence of Ni^{3+} ions has been established in the NiO reagent. On the other hand, oxidation of NiO to Ni_2O_3 is not inhibited if the synthesis is performed in the air, and the common high-temperature solid-state route in the air may cause a departure of the nominal $NiCr_2O_4$ composition. The substitution of the Cr^{3+} sites by Ni^{3+} ions looks favorable due to identical charges and similar ionic radii of these ions (0.615 Å for Cr^{3+} and 0.600 Å for Ni^{3+} in six-fold coordination [34]).

The electronic configuration of Ni^{3+} ions ($3d^8$, $t_{2g}^5 e_g^2$ in the cubic-symmetry crystal field) is different from that of the substituted Cr^{3+} ions ($3d^8$, t_{2g}^3). Anyway, the incorporation of the Ni^{3+} ions to the Cr^{3+} sites creates the local lattice distortions and therefore can easily affect the temperature of the orbital ordering, most probably decreasing its value. The pyrochlore-like structure of the B-site sublattice is the subject to magnetic frustration [35], which undoubtedly is a part of the story of why the temperature of magnetic ordering in $NiCr_2O_4$ is as low as ~65 K. A difference in electronic configurations between the Cr^{3+} and Ni^{3+} ions disturbs the fine balance of exchange interactions within the B-sublattice which will lead to an increase of the long-range spin ordering temperature. This indeed is the case in our study: the lower the value of the cationic substitution degree x, the lower the Nèel temperature (Table 2, Figure 6). It is not so easy to discuss in simple terms the trend for the transverse antiferromagnetic transition temperature T_s. As a matter of fact, the lower the x value, the higher the T_s (Table 2, Figure 6).

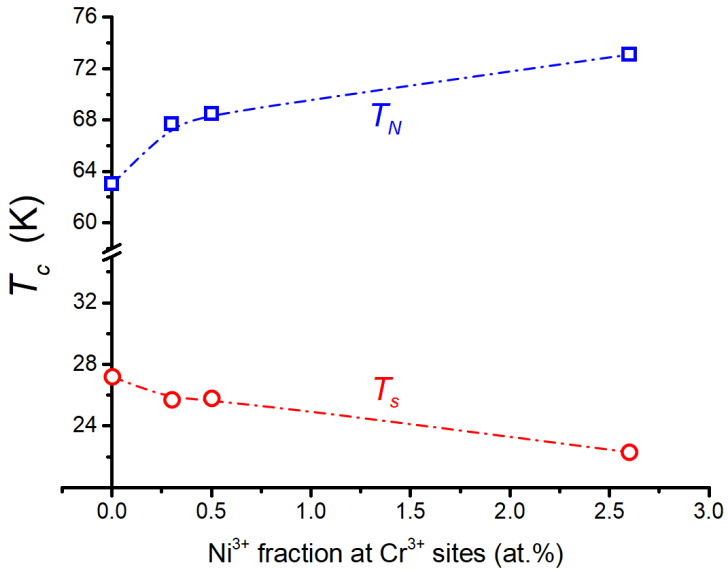

Figure 6. Dependence of the critical temperatures of magnetic orderings in powder samples of $NiCr_2O_4$ on the degree of Ni^{3+}-ion substitution for Cr^{3+} sites.

For sample III, which was obtained in a flow of argon, a significant part of the product was the metallic nickel (Table 1), and we expect a minimum of Ni^{3+} ions in its spinel fraction. This sample reveals the lowest Nèel temperature among our series and, probably, it is the lowest reported for this compound in the literature. Therefore, we suggest that the value of T_N = 63.0 K is most close to the intrinsic characteristic of the true $NiCr_2O_4$. We also propose that the Nèel temperature can serve as an easily accessible measure of departure of the composition of a compound obtained by whatever synthesis procedure from its nominal $NiCr_2O_4$.

7. Conclusions

To summarize, a series of seven $NiCr_2O_4$ powder samples have been produced following a conventional high-temperature solid-state synthesis route from the same NiO and Cr_2O_3 compounds. The influence of synthesis conditions, in particular the atmosphere in an oven chamber, on the phase composition of a product and magnetic and structural properties of the spinel fraction was studied. We find that all three critical temperatures corresponding to the orbital ordering (T_{OO}), onsets of the ferrimagnetic state (T_N), and transverse spin arrangement (T_s) vary with the changing atmosphere. We propose that Ni^{3+} ions that either occur in initial NiO or form during synthesis substitute for the Cr^{3+} ions in the octahedral B-sites of the spinel. Such substitution disturbs crystal lattice and dilutes the pyrochlore-like B-site magnetic sublattice and causes thus the shifts of the critical temperatures. The sample produced under an inert flowing Ar-gas atmosphere reveals the lowest Nèel temperature T_N = 63.0 K and the highest T_s = 27.2 K. In our opinion, the value of the Nèel temperature can serve as a measure of a departure of a sample composition from the nominal $NiCr_2O_4$. A study of the structural phase transition associated with an orbital ordering in the A-site Ni^{2+}-ion sublattice revealed the coexistence of cubic and tetragonal symmetry phases in the temperature range of 288–313 K, indicating a distribution of the orbital ordering temperature over a sample volume.

Author Contributions: Conceptualization, R.B. and R.Y.; methodology, I.V., A.K. and M.C.; formal analysis, A.R., D.G., A.K. and M.C.; investigation, M.C, A.R., D.G. and A.K.; resources, D.T., R.Y.; writing—original draft preparation, R.B. and R.Y.; writing—review and editing, R.Y., R.B. and M.C.; visualization, R.B. and M.C.; supervision, R.Y., D.T. and R.B. All authors have read and agreed to the published version of the manuscript.

Funding: The reported studies were performed with support from the Russian Science Foundation, project No. 19-12-00244.

Data Availability Statement: Raw data are available on a reasonable request to the corresponding author.

Acknowledgments: Electron microscopy studies were performed at the Interdisciplinary Centre for Analytical Microscopy of Kazan Federal University.

Conflicts of Interest: The authors declare no conflict of interest.

References

1. Tsurkan, V.; von Nidda, H.-A.K.; Deisenhofer, J.; Lunkenheimer, P.; Loidl, A. On the complexity of spinels: Magnetic, electronic, and polar ground states. *Phys. Rep.* **2021**, *926*, 1–86. [CrossRef]
2. Sundaresan, A.; Ter-Oganessian, N.V. Magnetoelectric and multiferroic properties of spinels. *J. Appl. Phys.* **2021**, *129*, 060901. [CrossRef]
3. Krupicka, S.; Novak, P. Oxide spinels. In *Handbook of Feromagnetic Materials*; Wohlfarth, E.P., Ed.; North-Holland Publishing Company: Amsterdam, The Netherlands, 1982; Volume 3, pp. 189–304. ISBN 978-0-444-86378-2.
4. Hemberger, J.; Lunkenheimer, P.; Fichtl, R.; Von Nidda, H.-A.K.; Tsurkan, V.; Loidl, A. Relaxor ferroelectricity and colossal magnetocapacitive coupling in ferromagnetic $CdCr_2S_4$. *Nature* **2005**, *434*, 364–367. [CrossRef] [PubMed]
5. Lee, S.-H.; Broholm, C.; Ratcliff, W.; Gasparovic, G.; Huang, Q.; Kim, T.H.; Cheong, S.-W. Emergent excitations in a geometrically frustrated magnet. *Nature* **2002**, *418*, 856–858. [CrossRef] [PubMed]
6. Fritsch, V.; Hemberger, J.; Büttgen, N.; Scheidt, E.-W.; von Nidda, H.-A.K.; Loidl, A.; Tsurkan, V. Spin and Orbital Frustration in $MnSc_2S_4$ and $FeSc_2S_4$. *Phys. Rev. Lett.* **2004**, *92*, 116401. [CrossRef]

7. Fichtl, R.; Tsurkan, V.; Lunkenheimer, P.; Hemberger, J.; Fritsch, V.; von Nidda, H.-A.K.; Scheidt, E.-W.; Loidl, A. Orbital Freezing and Orbital Glass State in$FeCr_2S_4$. *Phys. Rev. Lett.* **2005**, *94*, 027601. [CrossRef]
8. Yusupov, R.V.; Cherosov, M.A.; Gabbasov, B.F.; Vasin, K.V.; Batulin, R.G.; Kiyamov, A.G.; Eremin, M.V. Magnetic Irreversibilities and Nonreciprocity of the Microwave Absorption of $FeCr_2O_4$ Spinel. *J. Exp. Theor. Phys. Lett.* **2022**, *115*, 167–173. [CrossRef]
9. Batulin, R.; Cherosov, M.; Kiiamov, A.; Zinnatullin, A.; Vagizov, F.; Tayurskii, D.; Yusupov, R. Synthesis and Single Crystal Growth by Floating Zone Technique of $FeCr_2O_4$ Multiferroic Spinel: Its Structure, Composition, and Magnetic Properties. *Magnetochemistry* **2022**, *8*, 86. [CrossRef]
10. Lee, S.-H.; Gasparovic, G.; Broholm, C.; Matsuda, M.; Chung, J.-H.; Kim, Y.-J.; Ueda, H.; Xu, G.; Zschack, P.; Kakurai, K.; et al. Crystal distortions in geometrically frustrated ACr_2O_4 (A = Zn,Cd). *J. Phys. Condens. Matter* **2007**, *19*, 145259. [CrossRef]
11. Klemme, S.; O'Neill, H.S.; Schnelle, W.; Gmelin, E. The heat capacity of $MgCr_2O_4$, $FeCr_2O_4$, and Cr_2O_3at low temperatures and derived thermodynamic properties. *Am. Miner.* **2000**, *85*, 1686–1693. [CrossRef]
12. Rasool, R.Z.; Nadeem, K.; Kamran, M.; Zeb, F.; Ahmad, N.; Mumtaz, M. Comparison of anomalous magnetic properties of non-collinear $CoCr_2O_4$ and $NiCr_2O_4$ nanoparticles. *J. Magn. Magn. Mater.* **2020**, *514*, 167225. [CrossRef]
13. Rathi, A.; Babu, P.; Rout, P.; Awana, V.; Tripathi, V.K.; Nagarajan, R.; Sivaiah, B.; Pant, R.; Basheed, G. Anomalous nano-magnetic effects in non-collinear spinel chromite $NiCr_2O_4$. *J. Magn. Magn. Mater.* **2018**, *474*, 585–590. [CrossRef]
14. Arima, T.-H.; Yamasaki, Y.; Goto, T.; Iguchi, S.; Ohgushi, K.; Miyasaka, S.; Tokura, Y. Spin–Lattice Coupling in Ferroelectric Spiral Magnets: Comparison between the Cases of (Tb,Dy)MnO_3 and $CoCr_2O_4$. *J. Phys. Soc. Jpn.* **2007**, *76*, 023602. [CrossRef]
15. Singh, K.; Maignan, A.; Simon, C.; Martin, C. $FeCr_2O_4$ and $CoCr_2O_4$ spinels: Multiferroicity in the collinear magnetic state? *Appl. Phys. Lett.* **2011**, *99*, 172903. [CrossRef]
16. Lee, K.B.; Jo, S.; Choi, H.; Lee, Y.-W.; Sohn, J.I. Boosting catalyst activity with high valency metal species through Fe doping on normal spinel $NiCr_2O_4$ for superior water oxidation. *Appl. Surf. Sci.* **2023**, *609*, 155326. [CrossRef]
17. Zhao, J.; Li, X.; Cui, G.; Sun, X. Highly-active oxygen evolution electrocatalyzed by an Fe-doped $NiCr_2O_4$ nanoparticle film. *Chem. Commun.* **2018**, *54*, 5462–5465. [CrossRef]
18. Xu, X.; Gao, J.; Hong, W. Ni-based chromite spinel for high-performance supercapacitors. *RSC Adv.* **2016**, *6*, 29646–29653. [CrossRef]
19. Gao, H.; Guo, J.; Li, Y.; Xie, C.; Li, X.; Liu, L.; Chen, Y.; Sun, P.; Liu, F.; Yan, X.; et al. Highly selective and sensitive xylene gas sensor fabricated from NiO/$NiCr_2O_4$ p-p nanoparticles. *Sens. Actuators B Chem.* **2018**, *284*, 305–315. [CrossRef]
20. Ptak, M.; Maczka, M.; Gągor, A.; Pikul, A.; Macalik, L.; Hanuza, J. Temperature-dependent XRD, IR, magnetic, SEM and TEM studies of Jahn–Teller distorted $NiCr_2O_4$ powders. *J. Solid State Chem.* **2013**, *201*, 270–279. [CrossRef]
21. Suchomel, M.R.; Shoemaker, D.P.; Ribaud, L.; Kemei, M.C.; Seshadri, R. Spin-induced symmetry breaking in orbitally ordered $NiCr_2O_4$ and $CuCr_2O_4$. *Phys. Rev. B* **2012**, *86*, 054406. [CrossRef]
22. Klemme, S.; van Miltenburg, J.C. Thermodynamic properties of nickel chromite ($NiCr_2O_4$) based on adiabatic calorimetry at low temperatures. *Phys. Chem. Miner.* **2002**, *29*, 663–667. [CrossRef]
23. Tomiyasu, K.; Hiraka, H.; Ohoyama, K.; Yamada, K. Resonance-Like Magnetic Excitations in Spinel Ferrimagnets $FeCr_2O_4$ and $NiCr_2O_4$ Observed by Neutron Scattering. *J. Phys. Soc. Jpn.* **2008**, *77*, 124703. [CrossRef]
24. Tomiyasu, K.; Kagomiya, I. Magnetic Structure of $NiCr_2O_4$ Studied by Neutron Scattering and Magnetization Measurements. *J. Phys. Soc. Jpn.* **2004**, *73*, 2539–2542. [CrossRef]
25. Prince, E. Structure of Nickel Chromite. *J. Appl. Phys.* **1961**, *32*, S68–S69. [CrossRef]
26. Bertaut, E.F.; Dulac, J. Application of representation analysis to the magnetic structure of nickel chromite spinel. *Acta Crystallogr. Sect. A* **1972**, *28*, 580–588. [CrossRef]
27. Zhu, C.; Yu, G.; Wang, L.; Yao, M.; Liu, F.; Kong, W. Dielectric relaxation and magnetodielectric effect in the spinel $NiCr_2O_4$. *J. Magn. Magn. Mater.* **2020**, *506*, 166803. [CrossRef]
28. Ma, J.; Garlea, V.O.; Rondinone, A.; Aczel, A.A.; Calder, S.; Cruz, C.D.; Sinclair, R.; Tian, W.; Chi, S.; Kiswandhi, A.; et al. Magnetic and structural phase transitions in the spinel compound $Fe_{1+x}Cr_{2-x}O_4$. *Phys. Rev. B* **2014**, *89*, 134106. [CrossRef]
29. Li, C.; Yan, T.; Zerihun, G.; Fu, Q.; Zhang, R.; Chen, X.; Huang, S.; Yuan, S. Magnetization reversal induced by Mn substitution in spinel chromite $NiCr_2O_4$. *J. Am. Ceram. Soc.* **2018**, *101*, 5571–5577. [CrossRef]
30. Barman, J.; Ravi, S. Magnetization reversal and tunable exchange bias behavior in Mn-substituted $NiCr_2O_4$. *J. Mater. Sci.* **2018**, *53*, 7187–7198. [CrossRef]
31. Mohantya, P.; Prinsloo, A.R.E.; Sheppard, C.J.; Roos, W.D. Effect of Fe Substitution on Structural and Magnetic Properties of $NiCr_2O_4$. *Acta Phys. Pol. A* **2018**, *133*, 574–577. [CrossRef]
32. Cherosov, M.A.; Zinnatullin, A.L.; Batulin, R.G.; Kiiamov, A.G.; Yusupov, R.V.; A Tayurskii, D. Mössbauer effect study of a polycrystalline $Fe_{1+x}Cr_{2-x}O_4$ spinel grown by solid-state synthesis. *J. Physics: Conf. Ser.* **2022**, *2164*, 012067. [CrossRef]
33. Javed, A.; Szumiata, T.; Sarwar, A.; Fatima, T. Structure and Mössbauer spectroscopy studies of $Ni_{0.5}Zn_{0.5}NdFe_{2-x}O_4$ ($0.00 \leq x \leq 0.10$) ferrites. *Mater. Chem. Phys.* **2018**, *221*, 99–107. [CrossRef]

34. Shannon, R.T.; Prewitt, C.T. Revised values of effective ionic radii. *Acta Crystallogr. Sect. B Struct. Crystallogr. Cryst. Chem.* **1970**, *26*, 1046–1048. [CrossRef]
35. Yokaichiya, F.; Krimmel, A.; Tsurkan, V.; Margiolaki, I.; Thompson, P.; Bordallo, H.N.; Buchsteiner, A.; Stüßer, N.; Argyriou, D.N.; Loidl, A. Spin-driven phase transitions in $ZnCr_2Se_4$ and $ZnCr_2S_4$ probed by high-resolution synchrotron x-ray and neutron powder diffraction. *Phys. Rev. B* **2009**, *79*, 064423. [CrossRef]

Disclaimer/Publisher's Note: The statements, opinions and data contained in all publications are solely those of the individual author(s) and contributor(s) and not of MDPI and/or the editor(s). MDPI and/or the editor(s) disclaim responsibility for any injury to people or property resulting from any ideas, methods, instructions or products referred to in the content.